Available online at www.sciencedirect.com
SCIENCE DIRECT®
Engineering Applications of Artificial Intelligence 18 (2005) 731–744
Engineering Applications of
ARTIFICIAL
INTELLIGENCE
www.elsevier.com/locate/engappai

A cellular automaton for the propagation of circular fronts and its applications

G.Ch. Sirakoulis*, I. Karafyllidis, A. Thanailakis

Democritus University of Thrace, Department of Electrical and Computer Engineering, Laboratory of Electrical and Electronic Materials Technology, GR-671 00 Xanthi, Greece

Received 14 February 2004; received in revised form 19 December 2004; accepted 20 December 2004
Available online 8 March 2005

Abstract

Artificial intelligence techniques are widely used to solve complicated manufacturing and fabrication process problems in today's industrial world. Cellular automata (CAs) have been applied numerous times as an evolvable technique to the solution of some of the aforementioned complicated problems with great success due to their inherent parallelism, structural locality, regularity and modularity. One of the most difficult problems that CAs dealt with in several cases (i.e. integrated circuit fabrication, pattern recognition and classification, computer aided design, machine vision, etc.) is the identification and the reproduction of circular fronts and shapes. In this paper a CA is used to propagate circular fronts. This CA has an extended Moore neighborhood and a relatively simple local rule based on Boolean operators. Simulation results of an integrated circuit fabrication process, namely chemical vapor deposition based on the proposed CA are also presented. These results were found to be in very good qualitative agreement with the experimental results published in the literature. Moreover, because of the CA's binary states and its local rule simplicity, the VLSI implementation of the proposed CA is straightforward.

Keywords: Cellular automata; Circular fronts; Simulation; Chemical vapor deposition

1. Introduction

Cellular automata (CAs) were first introduced by von Neumann (1966), who was thinking of imitating the behavior of a human brain in order to build a machine able to solve very complex problems. His ambitious project was to show that complex phenomena can in principle be reduced to the dynamics of many identical, very simple primitives, capable of interacting and maintaining their identity (Chopard and Droz, 1998). Following a suggestion by Ulam (1952), von Neumann adopted a fully discrete approach, in which space, time, and even the dynamical variables were defined to be discrete. Consequently, CAs are very effective in simulating physical systems and solving scientific problems, because they can capture the essential features of systems where global behavior arises from the collective effect of simple components which interact locally (Calidona et al., 2002; Feynman, 1982; Wolfram, 1986). Nontrivial CAs are obtained whenever the dependence on the values at each site is nonlinear, as when the system exhibits some form of "material growth". As a result, any physical system satisfying differential equations may be approximated as a CA, by introducing finite differences and discrete variables (Bialynicki-Birula, 1994; Chen et al., 1990; Omohundro, 1984; Toffoli, 1984a; Vichniac, 1984; Wolfram, 1986).

During the following 60 years of existence, CAs have been developed and used in many different fields (Chopard and Droz, 1998; Preston and Duff, 1984). One of the most complex problems that CAs dealt

*Corresponding author. Tel.: +30 25410 79959; fax: +30 25410 29813.
E-mail address: gsirak@ee.duth.gr (G.Ch. Sirakoulis).

0952-1976/$ - see front matter © 2005 Elsevier Ltd. All rights reserved.
doi:10.1016/j.engappai.2004.12.008

with is the identification of circular shapes and the propagation of circular fronts. The number of targeted applications is extremely high varying from integrated circuit (ICs) fabrication processes, such as oxidation (Sirakoulis et al., 1999), chemical vapor deposition (Karafyllidis et al., 1998), to pattern recognition and identification of circular objects (Preston and Duff, 1984), to inspection tasks of circular objects such as tablets in pharmaceutical industry (Sirakoulis et al., 2001), to computer aided design (Karafyllidis et al., 1998; Preston and Duff, 1984), to machine vision and geometrical shape recognition (Karafyllidis et al., 1997; Preston and Duff, 1984), to patterns of growth (Chopard and Droz, 1998; Preston and Duff, 1984), and to several else not being able to mention here because of their extremely great number. As a result the need of CAs that are both space and time efficient to propagate circular fronts in order to produce, reconstruct and identify circular shapes and objects, with the minimum need of computational tasks, remains high.

The CAs models presented so far in the literature suffer from the drawback that the shape of the cells propagates in one way or another into the macroscopic scales, and thus leading to anisotropic wave propagation (Markus, 1991; Schönfisch, 1995). Several models have been proposed to overcome the anisotropy problem in CAs (Markus, 1991; Fast and Efimov, 1991; Kurrer and Schulten, 1991). Weimar et al. (1992) have considered simple threshold CAs with an extended Moore neighborhood. They found that the horizontal (vertical) speed depends on a threshold, and it is always a natural number, while the diagonal speed assumes values which are multiples of $\sqrt{2}/2$. Quantitatively these two speeds can be close together or very distinct. Although these workarounds remove the problem of anisotropy, as far as practical modelling is concerned, it should be noted that these models are characterized by extreme mathematical complexity and demand very large computational power and equally large computational time in order to produce simulation results (Delorme et al., 1999). The difficulties, arising from the implementation of the above models, and the existence of complex boundary conditions result in the requirement for extensive calculations and, therefore, long processing times. Karafyllidis et al. proposed some models that overcome only partially the problem of extensive calculations and simulate physical systems and processes of both microscopic and macroscopic level, such as IC fabrication processes (Karafyllidis et al., 1998; Sirakoulis et al., 1999), forest fire spreading (Karafyllidis, 2004), and modeling of epidemic propagation (Sirakoulis et al., 2000). The CA operation principles were generalized using continuous state space. CA cell states assume values between [0,1], and the CA local rule is expressed with the help of numerical operators (+, −, * and /). However, Delorme et al. (1999) have proved that complex high-level mathematical tools are needed for the geometrical construction of circular wave fronts using CAs with binary state space.

In this paper, a CA model with binary state space that successfully produces and propagates accurate circular fronts is presented for the first time. The proposed CA is characterized by an "extended" Moore neighborhood, i.e. the Moore neighborhood is extended to a 7×7 cell neighborhood shown in Fig. 1. A relatively simple local CA rule is applied, using AND and OR Boolean operators. This CA is able to construct and propagate accurate circular fronts. The proposed CA does not only succeeds a mere numerical agreement with a physical system/process, but also attempts to match the simulated system's own structure, its topology, its circular symmetries and, in short, everyone of its "deep" properties fulfilling the aforementioned criteria of circular front propagation. Furthermore, on account of the assumed CA's binary state space, its VLSI implementation is straightforward. As a result, the proposed binary CA could serve as a basis for the VLSI implementation of the aforementioned CA algorithms (Karafyllidis, 2004; Karafyllidis et al., 1998; Sirakoulis et al., 1999, 2000). These VLSI implementations lead to dedicated CA processors that execute the CA algorithms, and they can be designed using commercially available VLSI CAD tool systems.

The inherent parallelism of the proposed CA and its easy VLSI implementation make it suitable for real-time applications in the fields of semiconductor

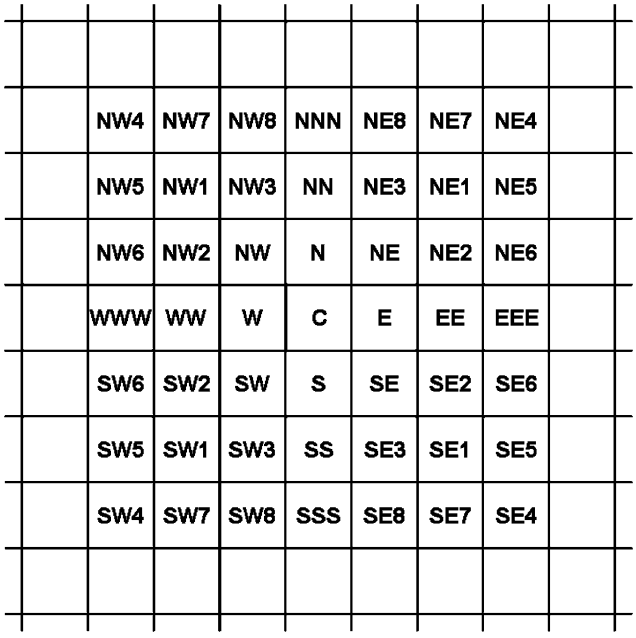

Fig. 1. "Extended" Moore neighborhood, i.e. the Moore neighborhood formed by (i, j) cell and its eight neighbors, is extended to a 7×7 cell neighborhood.

manufacturing, industrial engineering, pattern recognition, computer aided design, etc. In order to test the proposed CA in a actual problem of industrial engineering, numerical simulations of an integrated circuit fabrication process, namely chemical vapor deposition (CVD), were carried out. The simulations results produced by the propagation of the CA global state were compared successfully with other known models and were found to be in very good qualitative agreement with the experimental results found in the literature.

The paper is organized as follows: in Section 2, all the necessary background on CAs is given. The proposed CA is described in Section 3. This CA is tested under several grids and different initial conditions, in order to verify its ability to produce accurate circular fronts. A simulation paradigm of the CVD process, based on "material" wave propagation using the previously described CA, is given in Section 4. Finally, the conclusions drawn are presented in Section 5.

2. Cellular automata

CAs are models of physical systems, where space and time are discrete and interactions are local (von Neumann, 1966). In this section a more formal definition of a CA will be presented (Chopard and Droz, 1998). In general, a CA requires:

(i) a regular lattice of cells covering a portion of a d-dimensional space;
(ii) a set $\boldsymbol{C}(\vec{r},t)=\{C_1(\vec{r},t),C_2(\vec{r},t),\ldots,C_m(\vec{r},t)\}$ of variables attached to each site $\vec{r}$ of the lattice giving the local state of each cell at the time $t=0, 1, 2, \ldots$;
(iii) a rule $\boldsymbol{R}=\{R_1,R_2,\ldots,R_m\}$ which specifies the time evolution of the states $C(\vec{r},t)$ in the following way:

$$C_j(\vec{r},t+1)=R_j(\boldsymbol{C}(\vec{r},t),\boldsymbol{C}(\vec{r}+\vec{\delta}_1,t),\boldsymbol{C}(\vec{r}+\vec{\delta}_2,t),\ldots,\boldsymbol{C}(\vec{r}+\vec{\delta}_q,t)), \quad (1)$$

where $\vec{r}+\vec{\delta}_k$ designate the cells belonging to a given neighborhood of cell $\vec{r}$.

In the above definition, the rule $\boldsymbol{R}$ is identical for all sites, and it is applied simultaneously to each of them, leading to a synchronous dynamics. It is important to notice that the rule is homogeneous, i.e. it does not depend explicitly on the cell position $\vec{r}$. However, spatial (or even temporal) inhomogeneities can be introduced by having some $C_j(\vec{r})$ systematically at 1, in some given locations of the lattice, to mark particular cells for which a different rule applies. Furthermore, in the above definition, the new state at time $t+1$ is only a function of the previous state at time t. It is sometimes necessary to have a longer memory and introduce a dependence on the states at time $t-1$, $t-2,\ldots,$ $t-k$. Such a situation is already included in the definition, if one keeps a copy of the previous state in the current state.

The neighborhood of cell $\vec{r}$ is the spatial region in which a cell needs to search in its vicinity. In principle, there is no restriction on the size of the neighborhood, except that it is the same for all cells. However, in practice, it is often made up of adjacent cells only. For two-dimensional CA, two neighborhoods are often considered: the von Neumann neighborhood, which consists of a central cell (the one which is to be updated) and its four geographical neighbors north, west, south and east. The Moore neighborhood contains, in addition, second nearest neighbors northeast, northwest, southeast and southwest, that is a total of nine cells. In practice, when simulating a given CA rule, it is impossible to deal with an infinite lattice. The system must be finite and have boundaries. Clearly, a site belonging to the lattice boundary does not have the same neighborhood as other internal sites. In order to define the behavior of these sites, the neighborhood is extending for the sites at the boundary. Extending of the neighborhood leads to various types of boundary conditions such as periodic (or cyclic), fixed, adiabatic or reflection (Chopard and Droz, 1998).

CAs have sufficient expressive dynamics to represent phenomena of arbitrary complexity, and at the same time can be simulated exactly by digital computers, because of their intrinsic discreteness, i.e. the topology of the simulated object is reproduced in the simulating device (Vichniac, 1984). The CA approach is consistent with the modern notion of unified space–time. In computer science, space corresponds to memory and time to processing unit. In CAs, memory (CA cell state) and processing unit (CA local rule) are inseparably related to a CA cell. Furthermore, as mentioned in introduction, CAs are an alternative to partial differential equations (Bialynicki-Birula, 1994; Chen et al., 1990; Danikas et al., 1996; Omohundro, 1984; Toffoli, 1984a; Vichniac, 1984; Wolfram, 1986), and they can easily handle complicated boundary and initial conditions, inhomogeneities and anisotropies. In addition, algorithms based on CAs run quickly on digital computers (Toffoli, 1984b). As models for physical systems, CAs have many limitations. They are classical systems and, therefore, they cannot represent quantum mechanical systems. CAs should not be used to simulate systems, where speeds are comparable to that of light, because of the anisotropy induced by the discrete space. Models based on CAs lead to algorithms which are fast when implemented on serial computers, because they exploit the inherent parallelism of the CA structure. These algorithms are also appropriate for implementation on massively parallel computers, such as the cellular automaton

machine (CAM) (de Garis, 1994; Toffoli, 1984b; Wilding et al., 1991).

3. The proposed binary CA

In this section, a binary CA that successfully produces accurate circular fronts is presented for the first time. The proposed CA is characterized by an "extended" Moore neighborhood, i.e. the Moore neighborhood, formed by (i, j) cell itself and the eight adjacent cells, is extended to a 7×7 cell neighborhood shown in Fig. 1. A relatively simple local CA rule is applied, using the AND and OR Boolean operators.

In order to justify the choice of the "extended" Moore neighborhood, the results of applying the OR rule on Von Neumann and Moore neighborhoods will be presented in this section. The evolution of a binary CA under the OR local rule using the Von Neumann neighborhood, is presented in Fig. 2(a). The OR local rule is given by

$$C_{i,j}^{t+1} = C_{i,j}^{t} \text{ OR } C_{i-1,j}^{t} \text{ OR } C_{i+1,j}^{t} \text{ OR } C_{i,j-1}^{t} \text{ OR } C_{i,j+1}^{t}. \quad (2)$$

The global state produced by the CA evolution is a time-extended rhomboid front. In Fig. 2(b) is presented the evolution of the same CA using the Moore neighborhood. The OR local rule is given by

$$C_{i,j}^{t+1} = C_{i,j}^{t} \text{ OR } C_{i-1,j}^{t} \text{ OR } C_{i+1,j}^{t} \text{ OR } C_{i,j-1}^{t} \text{ OR } C_{i,j+1}^{t} \text{ OR } C_{i-1,j-1}^{t} \text{ OR } C_{i-1,j+1}^{t} \text{ OR } C_{i+1,j-1}^{t} \text{ OR } C_{i+1,j+1}^{t}. \quad (3)$$

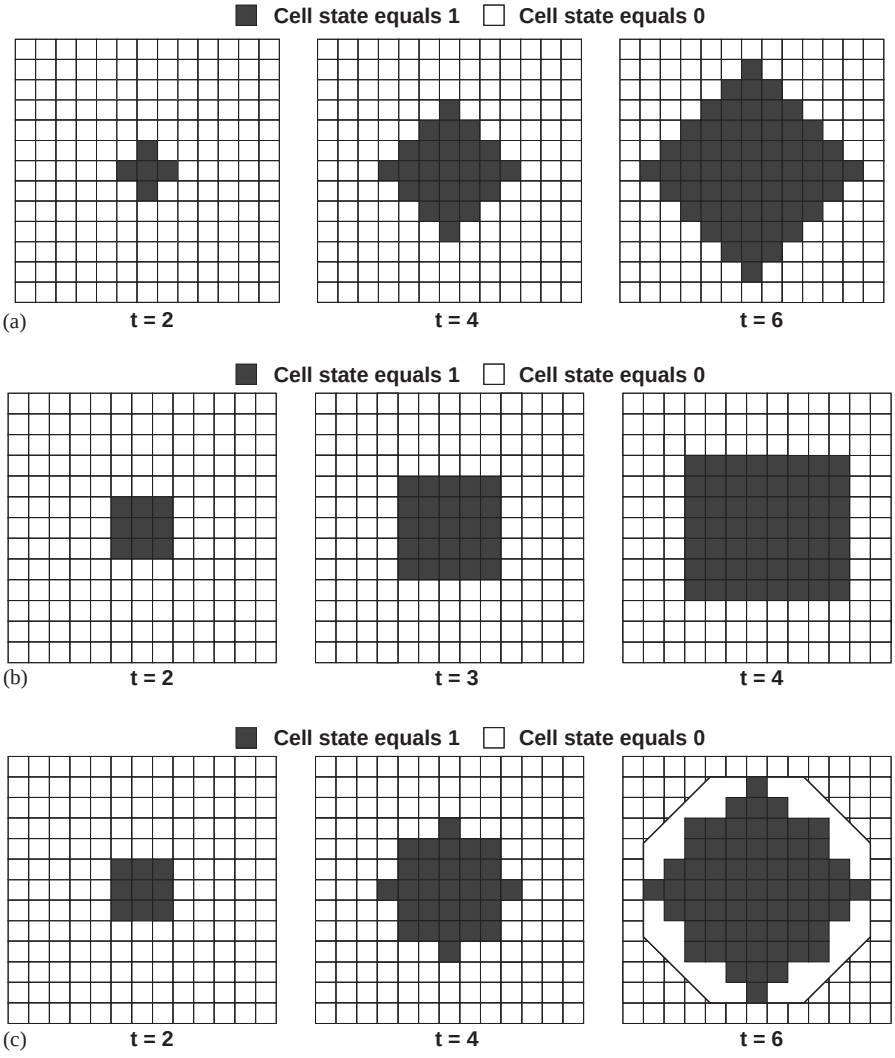

Fig. 2. (a) The evolution of a binary CA under the OR local rule using the Von Neumann neighborhood, (b) the evolution of a binary CA under the OR local rule using the Moore neighborhood, (c) the superposition of the above two figures results in a canonical octagonal front. For the construction of this canonical octagon, the OR CA local rule is applied using alternatively the Von Neumann and Moore neighborhood.

The global state produced by the CA evolution is now a time-extended square front. The superposition of these two figures results in a canonical octagonal front, presented in Fig. 2(c). This octagonal front will serve as the base for the construction of the circular front. For the construction of this canonical octagon, the OR CA local rule is applied using alternatively the Von Neumann and Moore neighborhood. The OR local rule is applied using the two neighborhoods at time steps given by

$$\begin{aligned} C_{i,j}^{t+1} &= C_{i,j}^{t} \text{ OR } C_{i-1,j}^{t} \text{ OR } C_{i+1,j}^{t} \text{ OR } C_{i,j-1}^{t} \\ &\quad \text{OR } C_{i,j+1}^{t} \text{ if } t = 8, 16, \ldots, t_n, t_n + 8, \ldots, \\ C_{i,j}^{t+1} &= C_{i,j}^{t} \text{ OR } C_{i-1,j}^{t} \text{ OR } C_{i+1,j}^{t} \text{ OR } C_{i,j-1}^{t} \text{ OR } C_{i,j+1}^{t} \\ &\quad \text{OR } C_{i-1,j-1}^{t} \text{ OR } C_{i-1,j+1}^{t} \text{ OR } C_{i+1,j-1}^{t} \\ &\quad \text{OR } C_{i+1,j+1}^{t} \text{ if } t = 5, 10, \ldots, t_m, t_m + 5, \ldots. \end{aligned} \tag{4}$$

In other words, the Von Neumann neighborhood is used every eight (8) evolution time steps, while the Moore neighborhood is used every five (5) evolution time steps. This way, the octagonal front is gradually transformed into a circular front, with the construction of exact curves on its sides. This is the reason why the CA neighborhood was extended to a 7×7 cell neighborhood, which from now on will be referred to as the "extended" Moore neighborhood (Fig. 1). The mathematical definition of the "extended" Moore neighborhood, i.e. the set of adjacent cells $B_{i,j}$ is given by the following equation:

$$B_{i,j} = \{C_{(i+n,j+m)}, \text{where } m, n \in \{-3, -2, -1, 0, 1, 2, 3\}\} \tag{5}$$

and it is presented in Fig. 1 with the help of the following equivalent relationships:

$$\begin{aligned} &C_{i,j} = \mathrm{C}, \quad C_{i-3,j-3} = \mathrm{NW}_4, \\ &C_{i-3,j-2} = \mathrm{NW}_7, C_{i-3,j-1} = \mathrm{NW}_8, \\ &C_{i-3,j} = \mathrm{NNN}, C_{i-3,j+1} = \mathrm{NE}_8, \\ &C_{i-3,j+2} = \mathrm{NE}_7, C_{i-3,j+3} = \mathrm{NE}_4, \\ &C_{i-2,j-3} = \mathrm{NW}_5, C_{i-2,j-2} = \mathrm{NW}_1, \\ &C_{i-2,j-1} = \mathrm{NW}_3, C_{i-3,j} = \mathrm{NN}, \\ &C_{i-2,j+1} = \mathrm{NE}_3, C_{i-2,j+2} = \mathrm{NE}_1, \\ &C_{i-2,j+3} = \mathrm{NE}_5, C_{i-1,j-3} = \mathrm{NW}_6, \\ &C_{i-1,j-2} = \mathrm{NW}_2, C_{i-1,j-1} = \mathrm{NW}, \\ &C_{i-1,j} = \mathrm{N}, C_{i-1,j+1} = \mathrm{NE}, \\ &C_{i-1,j+2} = \mathrm{NE}_2, C_{i-1,j+2} = \mathrm{NE}_6, \\ &C_{i,j-3} = \mathrm{WWW}, C_{i,j-2} = \mathrm{WW}, \\ &C_{i,j-1} = \mathrm{W}, C_{i,j+1} = \mathrm{E}, \\ &C_{i,j+2} = \mathrm{EE}, C_{i,j+3} = \mathrm{EEE}, \\ &C_{i+1,j-3} = \mathrm{SW}_6, C_{i+1,j-2} = \mathrm{SW}_2, \\ &C_{i+1,j-1} = \mathrm{SW}_5, C_{i+1,j} = \mathrm{S}, \\ &C_{i+1,j+1} = \mathrm{SE}, C_{i+1,j+2} = \mathrm{SE}_2, \\ &C_{i+1,j+3} = \mathrm{SE}_6, C_{i+2,j-3} = \mathrm{SW}_5, \\ &C_{i+2,j-2} = \mathrm{SW}_1, C_{i+2,j-1} = \mathrm{SW}_3, \\ &C_{i+2,j} = \mathrm{SS}, C_{i+2,j+1} = \mathrm{SE}_3, \\ &C_{i+2,j+2} = \mathrm{SE}_1, C_{i+2,j+3} = \mathrm{SE}_5, \\ &C_{i+3,j-3} = \mathrm{SW}_4, C_{i+3,j-2} = \mathrm{SW}_7, \\ &C_{i+3,j-1} = \mathrm{SW}_8, C_{i+3,j} = \mathrm{SSS}, \\ &C_{i+3,j+1} = \mathrm{SE}_8, C_{i+3,j+2} = \mathrm{SE}_7, \\ &C_{i+3,j+3} = \mathrm{SE}_4. \end{aligned} \tag{6}$$

It should be noted that the larger "extended" Moore neighborhood is used, i.e. when the indexes m and n take values greater than 3, the more exact curves will be produced using the proposed CA (Fast and Efimov, 1991; Weimar et al., 1992). The following instance-mathematical relationships are taken into consideration by the local CA rule, so that the central cell of the "extended" Moore neighborhood will change value to one, during the CA evolution, depending on the values of the adjacent neighboring cells:

$$\begin{aligned} C_{i,j}^{t+1} &= 1 \text{ IF}[(\mathrm{EEE} = 1 \& \mathrm{EE} = 1 \& \mathrm{E} = 1 \& \mathrm{S} = 1 \& \mathrm{SW} = 1 \& \mathrm{SW2} = 0 \& \mathrm{SW1} = 1) \\ &\quad \mathrm{OR}(\mathrm{EEE} = 1 \& \mathrm{EE} = 1 \& \mathrm{E} = 1 \& \mathrm{N} = 1 \& \mathrm{NW} = 1 \& \mathrm{NW2} = 0 \& \mathrm{NW1} = 1) \\ &\quad \mathrm{OR}(\mathrm{WWW} = 1 \& \mathrm{WW} = 1 \& \mathrm{W} = 1 \& \mathrm{N} = 1 \& \mathrm{NE} = 1 \& \mathrm{NE2} = 0 \& \mathrm{NE1} = 1) \\ &\quad \mathrm{OR}(\mathrm{WWW} = 1 \& \mathrm{WW} = 1 \& \mathrm{W} = 1 \& \mathrm{S} = 1 \& \mathrm{SE} = 1 \& \mathrm{SE2} = 0 \& \mathrm{SE1} = 1) \\ &\quad \mathrm{OR}(\mathrm{NNN} = 1 \& \mathrm{NN} = 1 \& \mathrm{N} = 1 \& \mathrm{W} = 1 \& \mathrm{SW} = 1 \& \mathrm{SW3} = 0 \& \mathrm{SW1} = 1) \\ &\quad \mathrm{OR}(\mathrm{NNN} = 1 \& \mathrm{NN} = 1 \& \mathrm{N} = 1 \& \mathrm{E} = 1 \& \mathrm{SE} = 1 \& \mathrm{SE3} = 0 \& \mathrm{SE1} = 1) \\ &\quad \mathrm{OR}(\mathrm{SSS} = 1 \& \mathrm{SS} = 1 \& \mathrm{S} = 1 \& \mathrm{W} = 1 \& \mathrm{NW} = 1 \& \mathrm{NW3} = 0 \& \mathrm{NW1} = 1) \\ &\quad \mathrm{OR}(\mathrm{SSS} = 1 \& \mathrm{SS} = 1 \& \mathrm{S} = 1 \& \mathrm{E} = 1 \& \mathrm{NE} = 1 \& \mathrm{NE3} = 0 \& \mathrm{NE1} = 1)]. \end{aligned} \tag{7}$$

$$\begin{aligned} &C_{i,j}^{t+1} \\ &= 1 \text{ IF } [(\mathrm{NW2} = 1 \& \mathrm{NW} = 1 \& \mathrm{N} = 1 \& \mathrm{NE} = 1 \& \mathrm{NE2} = 1) \\ &\mathrm{OR}\ (\mathrm{NW3} = 1 \& \mathrm{NW} = 1 \& \mathrm{W} = 1 \& \mathrm{SW} = 1 \& \mathrm{SW3} = 1) \end{aligned}$$

OR (SW2 = 1&SW = 1&S = 1&SE = 1&SE2 = 1)
OR (NE3 = 1&NE = 1&E = 1&SE = 1&SE3 = 1)].
(8)

$C_{i,j}^{t+1}$ = 1 IF[(NW2 = 1&W = 1&S = 1&SE3 = 1)
OR (SW2 = 1&W = 1&N = 1&NE3 = 1)
OR (NW3 = 1&N = 1&E = 1&SE2 = 1)
OR (SW3 = 1&S = 1&E = 1&NE2 = 1)]. (9)

$C_{i,j}^{t+1}$
= 1 IF [(NN = 1&N = 1&E = 1&SE = 1&SE3 = 1)
OR (NN = 1&N = 1&W = 1&SW = 1&SW3 = 1)
OR (WW = 1&W = 1&N = 1&NE = 1&NE2 = 1)
OR (WW = 1&W = 1&S = 1&SE = 1&SE2 = 1)
OR (SS = 1&S = 1&W = 1&NW = 1&NW3 = 1)
OR (SS = 1&S = 1&E = 1&NE = 1&NE3 = 1)
OR (EE = 1&E = 1&N = 1&NW = 1&NW2 = 1)
OR (EE = 1&E = 1&S = 1&SW = 1&SW2 = 1)], (10)

where the symbol & represents the logical Boolean operator AND. The above instance-mathematical relationships are depicted in Fig. 3(a)–(d), respectively. In all these figures, the adjacent cells, considered by the CA local rule, are connected with a black dotted line, marked with a small dot, and they have value one. On the other hand, the adjacent cells, considered by the CA local rule, in the same instance-mathematical relationship as the previous adjacent cells, but having value zero, are marked with a small gray star. The instance-mathematical relationships described by Eqs. (7)–(10) are depicted in Fig. 3(a)–(d), respectively. These relationships are applied as CA local rule at each time step of CA's evolution, together with the instance-mathematical relationship (6) applied as CA local rule when the time step is an integer multiple of the number 5 or 8. All these instance-mathematical relationships constitute the local rule of the binary CA proposed here.

The proposed CA was tested under several grids and different initial conditions, in order to establish, using statistical comparison calculations, its ability to construct exact circular fronts. The produced circular fronts were compared with the ones produced by CAs of continuous state space, presented analytically in

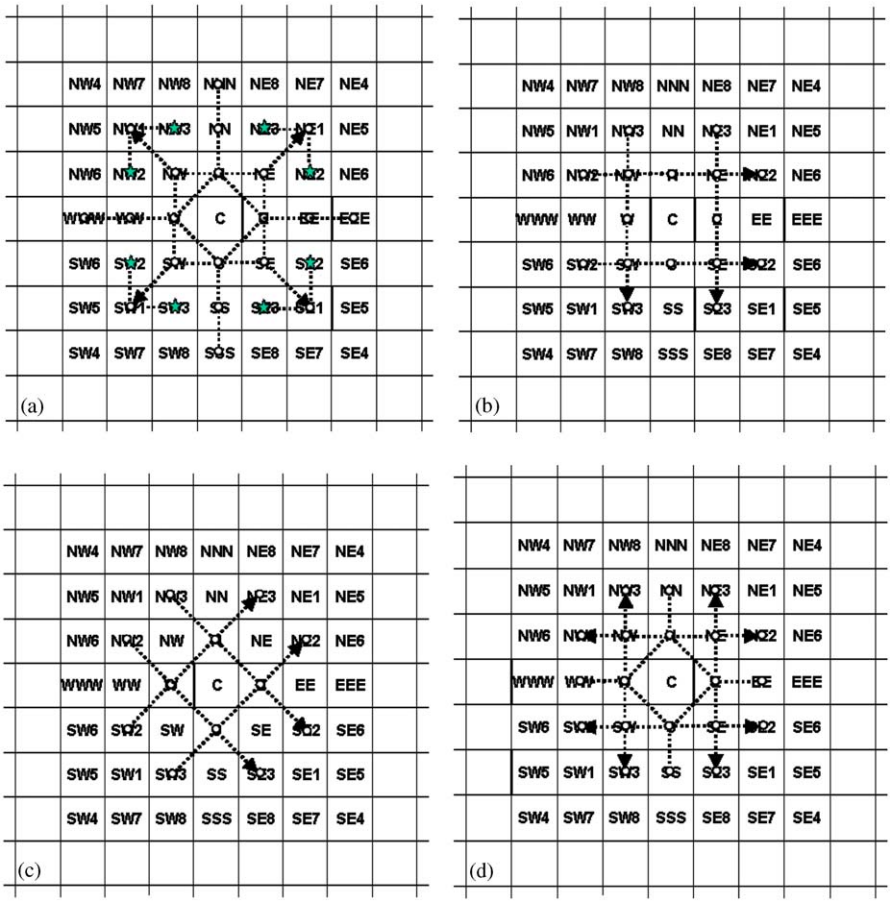

Fig. 3. The instance-mathematical relationships described by Eqs. (7)–(10) are depicted in (a)–(c), and (d), respectively. The adjacent cells, considered by the CA local rule, connected with a black dotted line and marked with a small dot have a value of one. The adjacent cells, considered by the CA local rule, connected with the same black dotted line and marked with a small gray star have a value of zero.

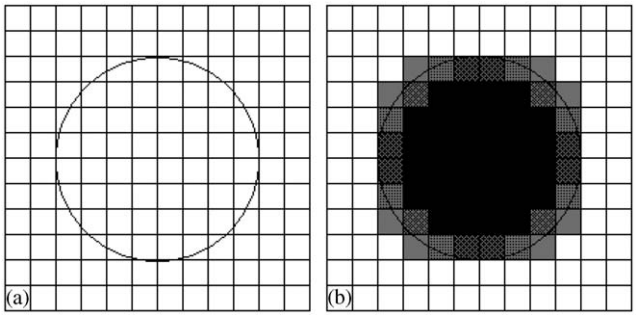

Fig. 4. Representation of circles on a CA lattice: (a) a circle on the CA lattice, and (b) the states of the CA cells. Black cells are located inside the circle and white cells outside the circle. The gray cells are located at the circumference. The gray color scales from dark gray to light gray as the cell state changes from 1 to 0.

(Karafyllidis, 2004; Karafyllidis et al., 1998; Sirakoulis et al., 1999, 2000, 2002). A brief discussion on CAs with continuous state space follows now.

Consider the circle on the CA lattice shown in Fig. 4(a). The CA cells that are located completely inside the circle are represented in Fig. 4(b) as black cells, whereas the cells that are located completely outside the circle are represented as white cells. Gray cells represent cells located partially inside and partially outside the circle. The cell state of a CA that produces circular fronts is given by

$$C_{i,j}^{t} = \frac{E_{\text{in}}}{E_{\text{t}}}, \tag{11}$$

where $C_{i,j}^{t}$ is the local state of the (i,j) cell, at time t, E_{in} is the cell area located inside the circle and E_t is the total cell area. Obviously a cell located completely inside the circle has state 1 and a cell located completely outside the circle has state 0. In Fig. 4(b), gray scales from dark gray to light gray as the cell state changes from 1 to 0. A CA local rule applied to a continuous state space CA, that produces circular fronts, is the following (Karafyllidis, 2004; Karafyllidis et al., 1998; Sirakoulis et al., 1999, 2000, 2001):

$$\begin{aligned} C_{i,j}^{t+1} = {} & C_{i,j}^{t} + (C_{i-1,j}^{t} + C_{i,j-1}^{t} + C_{i,j+1}^{t} + C_{i+1,j}^{t}) \\ & + 0.83(C_{i-1,j-1}^{t} + C_{i-1,j+1}^{t} \\ & + C_{i+1,j-1}^{t} + C_{i+1,j+1}^{t}), \end{aligned} \tag{12}$$

where $C_{i,j}^{t}$ and $C_{i,j}^{t+1}$ are the states of the (i,j) cell at times t and $t+1$, respectively. The circular fronts produced by this rule become smoother as the size of the CA lattice increases.

The calculations were made using the covered area of the grid at each time step, which is practically the number of cells with state one, at each evolution step of either the CA with continuous state space or the CA with binary state space, respectively. It should be noted that the comparison of covered grid areas of the two evolving CAs will be possible, if there is a common starting point, since the time steps needed to cover the same distance are different for each CA. Such a common starting point is the radius of the circular fronts produced, which should be the same for both CAs, in all cases. Furthermore, the finally produced circular fronts of the CA with continuous state space are normalized, i.e. the values of the CA grid cells are compared with the normalization value 0.5 so that, if they are greater than this value, they are equal to one, otherwise they are equal to zero, as described by the equation:

$$C_{i,j} = \begin{cases} 0 & \text{if } C_{i,j} < 0.5, \\ 1 & \text{if } C_{i,j} \geqslant 0.5. \end{cases} \tag{13}$$

This way, it is possible to compare the covered grid areas of the evolving CAs produced in each case. As a result, the CA with continuous state space and the CA with discrete (binary) state space were compared in producing circular wave fronts for different grids and, specifically, for grids of 50×50, 100×100, 150×150 and 200×200 cells, at different evolution time steps, for three different initial conditions. In particular, the following initial conditions were used for the two CAs: (a) from a central cell, i.e. from a point, (b) from three central cells located on a line, i.e. from a line, and (c) from five cells forming a rectangular angle, i.e. from an angle. Furthermore, the boundary conditions of the proposed CAs are chosen to be periodic, or zero, without any effect on the final results of the CAs' evolution that will be presented below.

In Fig. 5(a) and (b), the circular fronts produced by the evolution of the CA with continuous state space are presented, for different grids of 50×50, and 150×150 cells, at different time steps $t = 14$, and $t = 23$, respectively. In Fig. 5(c) and (d), the evolution results of the CA with discrete state space are presented, for different grids of 50×50, and 150×150 cells at different time steps $t = 14$, and $t = 23$, respectively. In all cases the central cell of each grid was set to state one. The results of evolution of the CAs studied are similar in all cases, as it is confirmed by the comparison of the covered areas, at different time steps. Notwithstanding that the calculations have been made at different time steps, for each of the two CAs, the circular fronts produced by the two CAs have exactly the same radius. The evolution of the two CAs is compared for the grid of 200×200 cells, and the results are presented in Fig. 8(a). Most of the statistical comparison calculations were done on a grid of 200×200 cells. As it is obvious from Fig. 8(a), the final difference between the covered areas of the two CAs is never greater than 10%.

Similarly, in Fig. 6(a) and (b), the circular fronts, produced by the evolution of the CA with continuous state space, are presented for different grids of

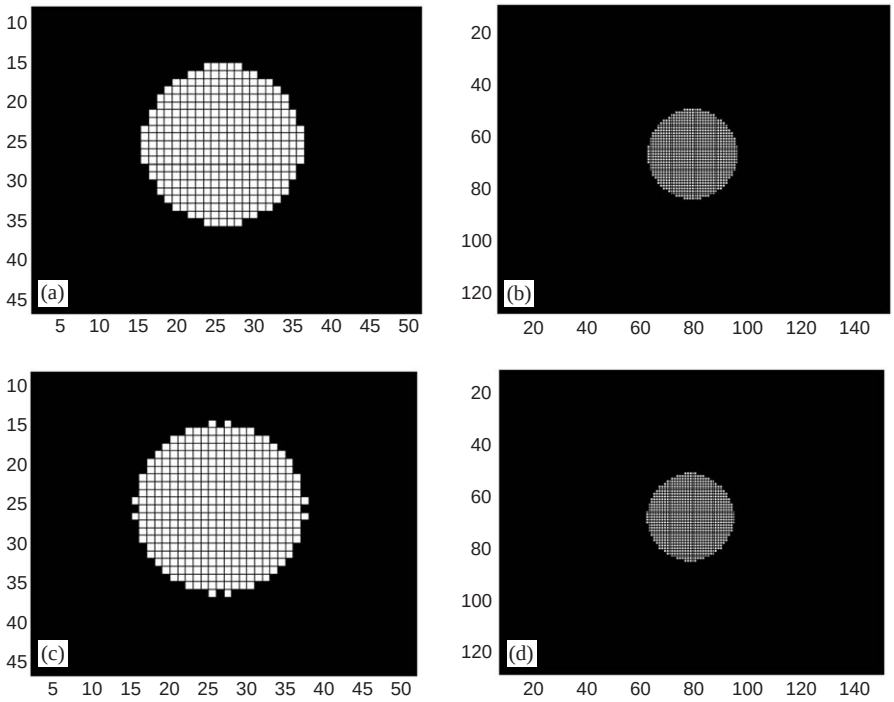

Fig. 5. Circular fronts, produced by the evolution of the CA with continuous state space, are presented for different grids of: (a) 50×50, and (b) 150×150 cells, at different time steps $t = 14$, and $t = 23$, respectively. Circular fronts, produced by the evolution of the CA with discrete state space, are presented for different grids of: (c) 50×50, and (d) 150×150 cells, at different time steps $t = 25$, and $t = 36$, respectively. In all cases, the central cell of each grid was set to state one.

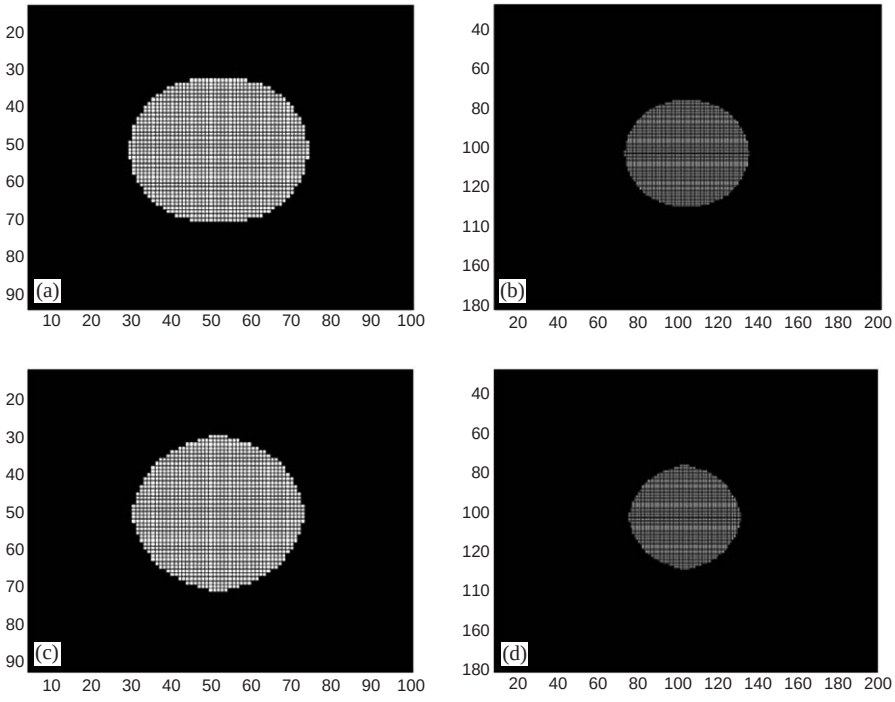

Fig. 6. Evolution results of the CA with continuous state space for different grids of: (a) 100×100, and (b) 200×200 cells, at different time steps $t = 24$, and $t = 35$, respectively. Evolution results of the CA with discrete state space for different grids of: (c) 100×100, and (d) 200×200 cells, at different time steps $t = 35$ and $t = 48$, respectively. In all cases, the three central cells of each grid, located on a line, were set to state one.

100×100, and 200×200 cells, at different time steps $t = 24$, and $t = 35$, respectively. In Fig. 6(c) and (d), the evolution results of the CA with discrete state space, are presented for different grids of 100×100, and 200×200 cells, at different time steps $t = 35$, and $t = 48$, respectively. In all cases, the three central cells of each grid, located on a line, were set to state one. The evolution results obtained from the CAs studied are similar in all cases, as it is confirmed by comparison of the covered areas, at different time steps. Notwithstanding, that the calculations have been made on different time steps, for each of the two CAs, the circular fronts produced by the compared two CAs, have equal horizontal and vertical radii, respectively. The evolution of the two CAs is compared for the grid of 200×200 cells, and the results are presented in Fig. 8(b). Most of the statistical comparison calculations were done on a grid of 200×200 cells. As it is obvious from Fig. 8(b), the final difference between the covered areas of the two CAs is never greater than 10%.

Finally, in Fig. 7(a)–(c), the evolution results of the CA with continuous state space are presented, for different grids of 100×100, 150×150 and 200×200 cells, at different time steps $t = 13$, $t = 22$ and $t = 25$, respectively. In Fig. 7(d)–(f), the evolution results of the CA with discrete state space are presented, for different grids of 100×100, 150×150 and 200×200 cells, at different time steps $t = 20$, $t = 32$ and $t = 36$,

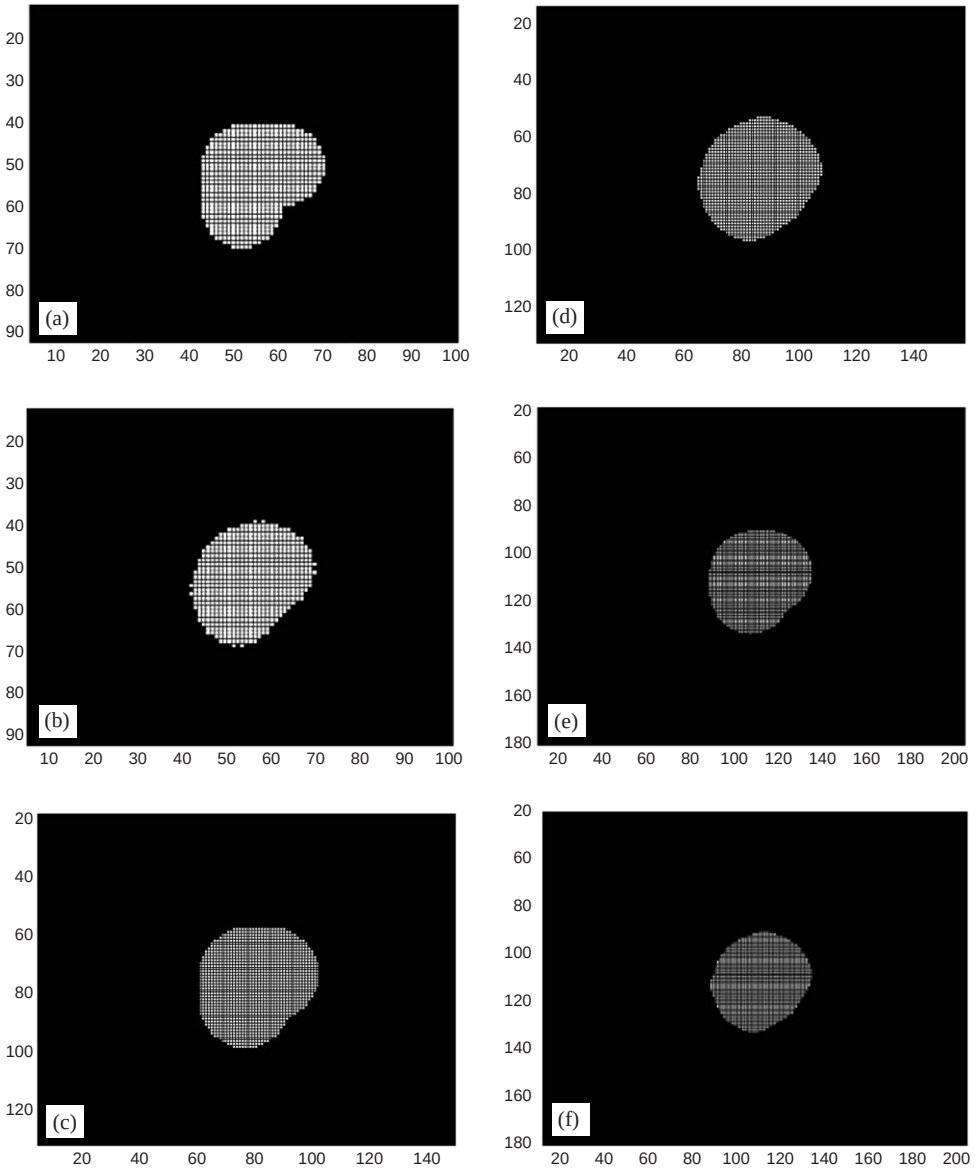

Fig. 7. Evolution results of the CA with continuous state space for different grids of: (a) 100×100, (b) 150×150, and (c) 200×200 cells, at different time steps $t = 13$, $t = 22$, and $t = 25$, respectively. Evolution results of the CA with discrete state space for different grids of: (d) 100×100, (e) 150×150, and (f) 200×200 cells, at different time steps $t = 20$, $t = 32$, and $t = 36$, respectively, and with five central cells of each grid that form a rectangular angle, exactly the same as in the case of the continuous CA, and have state one.

respectively, and with five central cells of each grid that form a rectangular angle, exactly the same as in the case of the continuous CA, and have state one. The evolution results obtained form the CAs studied are similar in all cases, as it is confirmed by the comparison of the covered areas at different time steps. Notwithstanding, that the calculations have been made on different time steps for each of the two CAs. It should be noted that the rectangular angle, formed by the five initial central cells, has southeastern direction, i.e. the angle extends to east at the horizontal x-axis and to south at the vertical y-axis. As a result the south and east radii of the circular fronts, calculated from the center of the CA grid, are going to be equal. Furthermore, in the same way, the north and west radii of the circular fronts produced, calculated from the center of the CA grid, are going to be equal too. The aforementioned radii are the ones that will be used on the statistical comparison calculation of the circular fronts produced. The evolution of the two CAs is compared, for the grid of 200×200 cells, and the results are presented in Fig. 8(c). As before, most of the statistical comparison calculations were done on a grid of 200×200 cells. As it is obvious from Fig. 8(c), the final difference between the covered areas of the two CAs is never greater than 10%.

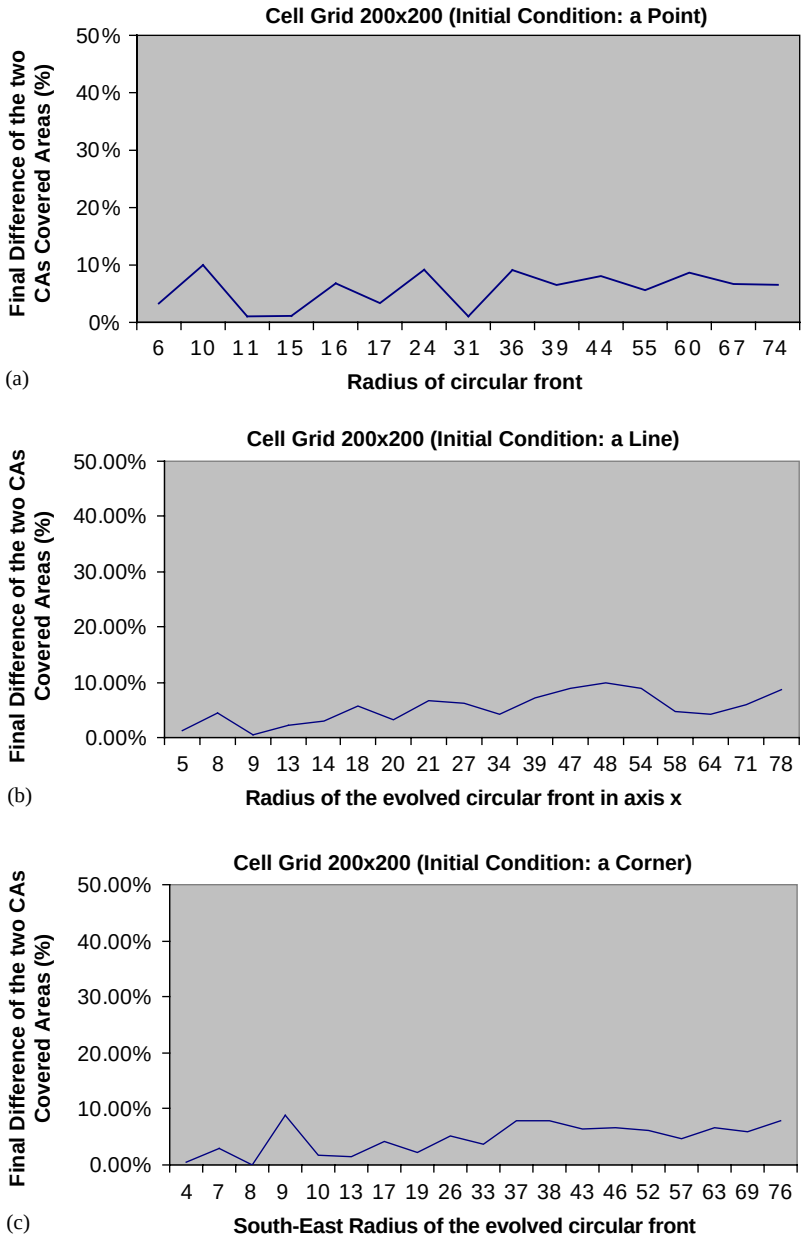

Fig. 8. The evolution of the two CAs is compared for the grid of 200×200 cells, with the following initial conditions: (a) a point, (b) a line, and (c) a rectangular angle.

4. The simulation paradigm of chemical vapor deposition process

In this section an application example of the proposed CA on the simulation of the CVD IC fabrication process is presented. The simulations to be presented are only a few of the several possible cases manipulated by the CA. However, these simulations are characteristic working cases of the CVD process and the deposition simulation profiles obtained are in very good qualitative agreement with the experimental and simulation results found in the literature.

CVD has been an important technology for the deposition of thin films on silicon wafers, from the earliest days of the microelectronics industry (Meyyappan, 1995). Modelling of the CVD process has seen increasing use of simulation techniques, while the most deposition models are based on two mathematical formulations: the formulation of characteristic trajectories (Tazawa et al., 1992), and the formulation of the level set function (Sethian, 1985). Both mathematical formulations result in boundary advancement similar to that of Huygens' waves, i.e. the points of the old boundary are supposed to be Huygens' sources that emit circular "material" waves and the new boundary is the envelope of these waves (Sethian, 1985; Tazawa et al., 1992). This boundary advancement is depicted in Fig. 9, which shows a uniform (CVD) deposition over a rectangular trench. All circles have centers on the old boundary. After a time step (unit time), a boundary point advances by a distance equal to the surface movement velocity. Hence, the circle radius is equal to this velocity. The boundary between deposited material and air is also called "deposition profile", or "profile". More details about the CDV process can be found in the literature (Ikegawa and Kobayashi, 1989; Meyyappan, 1995; Sethian, 1985; Tazawa et al., 1992).

When the CA cells are to be used as Huygens' sources, the problem of constructing circular fronts on the rectangular CA lattice emerges. The cell state of the CA, on the lattice of which the equations of either of the two mathematical formulations are solved, is

$$S_{i,j}^t = \{B_{i,j}^t, V_{i,j}^t, C_{i,j}^t\}, \tag{14}$$

where $C_{i,j}^t$ is given by Eq. (11), and it is calculated using Eq. (12). This ensures that circular fronts will be produced. The radius of the circular front that will be produced by the (i, j) cell at time step t is determined by $V_{i,j}^t$, which is the surface movement velocity at the center of the (i, j) cell at time step t. The surface movement velocity can be determined using any one of the mathematical formulations found in the literature. Only cells located at the boundary can produce circular fronts. A CA cell is a boundary cell:

$$\begin{aligned}\text{IF}\{C_{i,j}^t = 1 \text{ AND } [(C_{i,j+1}^t\langle 1) \text{ OR } (C_{i,j-1}^t\langle 1)\\ \text{OR } (C_{i+1,j}^t\langle 1) \text{ OR } (C_{i-1,j}^t\langle 1)\\ \text{OR } (C_{i-1,j-1}^t\langle 1) \text{ OR } (C_{i-1,j+1}^t\langle 1)\\ \text{OR } (C_{i+1,j-1}^t\langle 1) \text{ OR } (C_{i+1,j+1}^t\langle 1)]\}.\end{aligned} \tag{15}$$

In other words, boundary cells are the black cells that have at least one gray or white cell as a neighbor, as presented in Fig. 4. $B_{i,j}^t$ is a one bit flag, and indicates if the (i, j) cell will be used as a Huygens' source at time step t. If the (i, j) cell is a boundary cell, then $B_{i,j}^t = 1$, and if not then $B_{i,j}^t = 0$. The cell will be used as a Huygens' source only if $B_{i,j}^t = 1$.

In the case of granule presence, the chemical kinetics is also described by the aforementioned mathematical formulations. To incorporate granules one more flag is added to the CA cell state:

$$S_{i,j}^t = \{D_{i,j}, B_{i,j}^t, V_{i,j}^t, C_{i,j}^t\}. \tag{16}$$

$D_{i,j}$ is a one bit flag indicating whether this cell belongs to the granule ($D_{i,j} = 1$) or not ($D_i j = 0$). If $D_{i,j} = 1$ the value of $C_{i,j}^t$ is not calculated. An analytical description of the continuous state space CA deposition simulator faithful to the underlying partial differential equations that describe the CVD process can be found in (Karafyllidis et al., 1998).

In Fig. 10 deposition simulation profiles obtained in the cases of: (a) a planar silicon surface, (b) a silicon ditch, (c) a silicon column, and (d) a silicon column with a defect are presented. These are working case simulations using the CA model proposed by Karafyllidis et al. (1998), and they are used for reasons of simplicity, convenience, and statistical comparison, to check the ability of the aforementioned CA to produce deposition profiles of the same accuracy with the ones presented in Fig. 10. The state space of the CA model for the deposition simulation has been chosen to be continuous in all Fig. 10, with the maximum simulation time and the maximum cell number for each grid side being 18 and 50, respectively, for all the aforementioned working cases studied.

All the cases of the simulated deposition process studied are depicted in Fig. 11, using this time the proposed CA with discrete (binary) state space. As mentioned in the previous section, the difference between the state spaces of the CA algorithms leads to different evolution times and different grid sizes. Consequently, the values of these algorithm parameters,

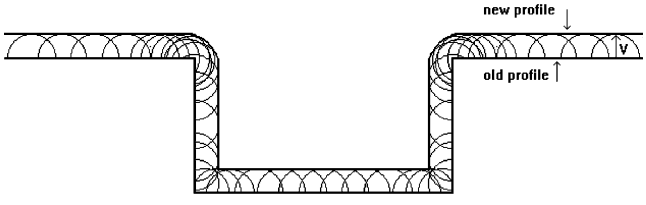

Fig. 9. Advancement of the CVD profile.

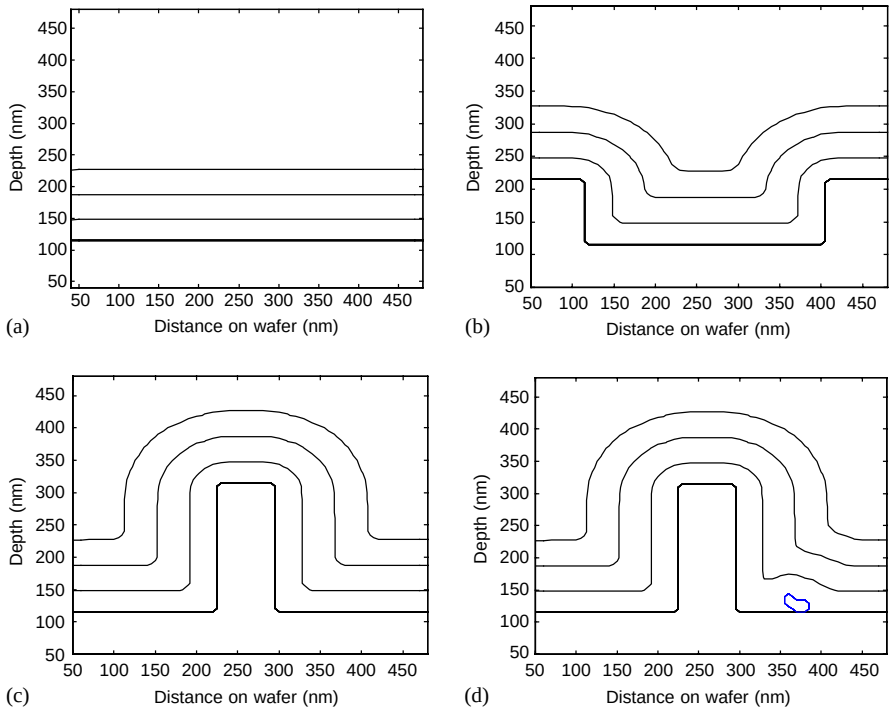

Fig. 10. Deposition simulation profiles obtained in the cases of: (a) a planar silicon surface, (b) a silicon ditch, (c) a silicon column, and (d) a silicon column with a defect, using a CA with continuous state space.

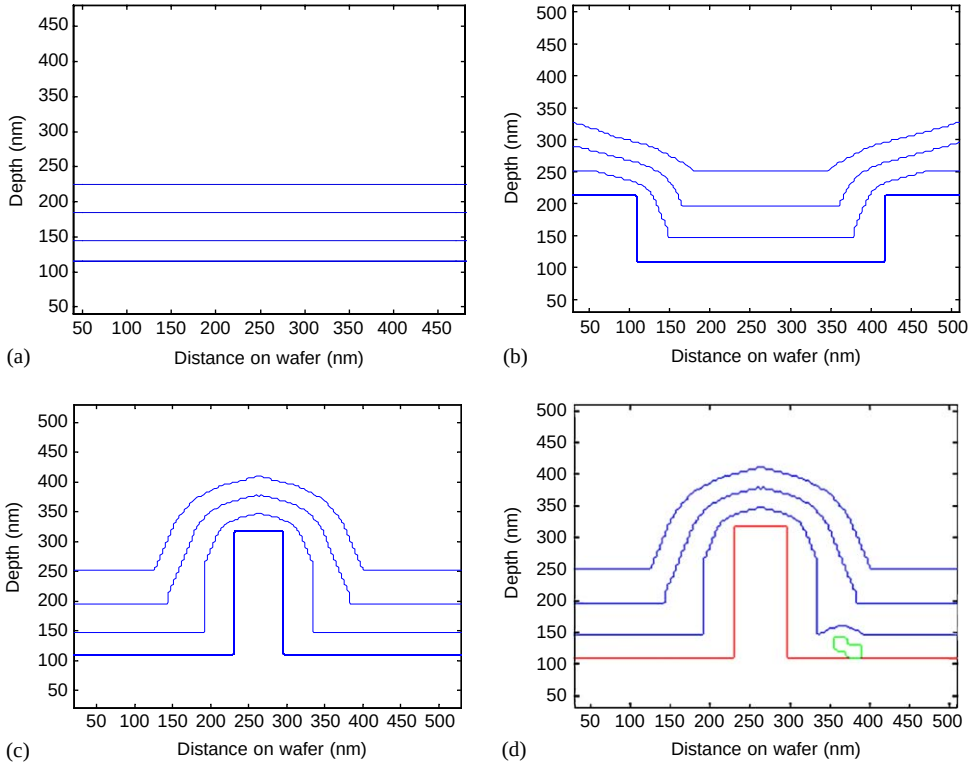

Fig. 11. Deposition simulation profiles in the cases of: (a) a planar silicon surface, (b) a silicon ditch, (c) a silicon column, and (d) a silicon column with a defect, obtained using the proposed binary CA.

in all working case simulations (a)–(d), should be slightly increased in the case of discrete state space, in order to simulate the deposition process with the same accuracy, as in case of continuous state space.

The time needed by the CA algorithm, in both cases, to produce successfully the simulation deposition profiles, increases very much as the maximum simulation time or/and the grid size are increased. As a result, the maximum simulation time and the maximum grid size are chosen to be 41 and 150, respectively, rather than to achieve the best combination of computational accuracy and computational time-memory, for all working cases (b)–(d), except (a). In case (a), the maximum simulation time and the maximum grid size are chosen to be 18 and 50, respectively, i.e. exactly the same as in case of simulating the deposition process using the continuous CA algorithm. The main difference between this case (a) and the other three cases (b)–(d) is induced by the lack of curvature in the simulation profiles obtained, arising from the planarity of silicon surface. The lack of curvature is less for the deposition profiles with high accuracy and similarity with those generated by the CA algorithm with continuous state space.

The comparison of simulation results on the deposition profiles in the cases of the CA presented by Karafyllidis et al. (Fig. 10) and the proposed CA in this paper (Fig. 11) leads to the conclusion that the aforementioned binary CA simulates very successfully the deposition process. The qualitative similarity between the deposition profiles of continuous and discrete state space is confirmed by the results of statistical comparison calculations of the deposition areas in both cases.

Indeed, in all working cases of deposition simulation, the final difference between the covered deposition areas of the two CAs is never greater than 9%. More specifically, in the case of Figs. 10(a) and 11(a) the final difference between the covered areas of the profiles produced is 8.40%, in the case of Figs. 10(b) and 11(b) it is 0.07%, in the case of Figs. 10(c) and 11(c) it is 1.45%, and in the case of Figs. 10(d) and 11(d) it is equal to 2.75%.

It should be mentioned that, in the case of the presented binary CA, the deposition covered area has been normalized, i.e. it has been divided by the normalization number 9 [the ratio of the product of binary CA grid sizes ($150 \times 150 = 22500$) to the product of continuous CA grid sizes ($50 \times 50 = 2500$)], in order to be compared with the deposition covered area in the case of the CA with continuous state space. Furthermore, in order to calculate the deposition covered area of the continuous CA, all the CA cell states are normalized after the production of the final deposition profiles, i.e. the values of the CA grid cells are compared with the normalization value 0.5, so that if they are greater than this value they are equal with the value one, otherwise they are equal with the value zero.

5. Conclusions

A CA algorithm with binary state space that successfully produces accurate circular fronts was presented for the first time. The proposed CA is characterized by an "extended" Moore neighborhood, while a relatively mathematical simple local CA rule is applied, using AND and OR Boolean operators. The inherent parallelism of the proposed CA and its easy VLSI implementation make it suitable for real-time applications in the fields of semiconductor manufacturing, industrial engineering, pattern recognition, computer aided design, etc. In order to test the proposed CA in an actual problem of industrial engineering, numerical simulations of an integrated circuit fabrication process, namely CVD, were carried out. The simulations results produced by the propagation of the CA global state were found to be in very good qualitative agreement with the experimental results published in the literature. Furthermore, on account of the assumed CA's binary state space, its VLSI implementation is straightforward. As a result, the proposed binary CA could serve as a basis for the VLSI implementation of the several CA algorithms. These VLSI implementations lead to dedicated CA processors that execute the CA algorithms, and they can be designed using commercially available VLSI CAD tool systems.

References

Bialynicki-Birula, I., 1994. Weyl, Dirac, and Maxwell equations on a lattice as unitary cellular automata. Physical Review D 49, 6920–6927.

Calidona, C.R., Di Gregorio, S., Magno Furnari, M., 2002. Mapping applications of cellular automata into applications of cellular automata networks. Computer Physics Communication 147, 724–728.

Chen, H., Matthaeus, W.H., Klein, L.W., 1990. Theory of multicolor lattice gas: a cellular automaton Poisson solver. Journal of Computational Physics 88, 433–466.

Chopard, B., Droz, M., 1998. Cellular Automata Modeling of Physical systems. Cambridge University Press, Cambridge.

Danikas, M.G., Karafyllidis, I., Thanailakis, A., Bruning, A.M., 1996. Simulation of electrical tree growth in solid dielectrics containing voids of arbitrary shape. Modelling Simulation Materials Sci. Eng. 4, 535–552.

de Garis, H., 1994. CAM-Brain: the genetic programming of an artificial brain which grows/evolves at electronic speeds in a cellular automata machine. Proceedings of first IEEE Conference on Evolutionary Computation, vol. 1. New York, USA, pp. 337–339.

Delorme, M., Mazoyer, J., Tougne, L., 1999. Discrete parabolas and circles on 2D cellular automata. Theoretical Computer Science 218 (2), 347–417.

Fast, V.G., Efimov, I.R., 1991. Stability of vortex rotation in an excitable cellular medium. Physica D 49, 75–81.

Feynman, R.P., 1982. Simulating physics with computers. International Journal of Theoretical Physics 21 (6/7), 467–488.

Ikegawa, M., Kobayashi, J., 1989. Description profile simulation using Monte Carlo method. Journal of Electrochemical Society 136, 2982–2989.

Karafyllidis, I., 2004. Design of a dedicated parallel processor for the prediction of forest fire spreading using cellular automata and genetic algorithms. Engineering Applications of Artificial Intelligence 17 (1), 19–36.

Karafyllidis, I., Ioannidis, A., Thanailakis, A., Tsalides, Ph., 1997. Geometrical shape recognition using a cellular automaton architecture and its VLSI implementation. Real-Time Imaging 3, 243–254.

Karafyllidis, I., Georgoulas, N., Haguel, P.I., Thanailakis, A., 1998. Simulation of deposition-topography granular distortion for TCAD. Modelling and Simulation Materials Science Engineering 6, 199–210.

Kurrer, C., Schulten, K., 1991. Propagation of chemical waves in discrete excitable media: anisotropic and isotropic wave fronts. In: Holden, A.V., Markus, M., Othmer, H.G. (Eds.), Nonlinear Wave Processes in Excitable Media. Plenum Press, New York, pp. 489–500.

Markus, M., 1991. Dynamics of a cellular automaton with randomly distributed elements. In: Arino, O., Axelrod, D.E., Kimmel, M. (Eds.), Mathematical Population Dynamics. Marcel Dekker, New Yok, pp. 413–434.

Meyyappan, M., 1995. Computational Modeling in Semiconductor Processing. Artech House, Boston, MA.

Omohundro, S., 1984. Modeling cellular automata with partial differential equations. Physica D 10 (1–2), 128–134.

Preston Jr., K., Duff, M.J.B., 1984. Modern Cellular Automata: Theory and Applications. Plenum Press, New York.

Schönfisch, B., 1995. Propagation of fronts in cellular automata. Physica D 80, 433–450.

Sirakoulis, G.Ch., Karafyllidis, I., Soudris, D., Georgoulas, N., Thanailakis, A., 1999. A new simulator for the oxidation process in integrated circuit fabrication based on cellular automata. Modelling and Simulation Material Science Engineering 7 (4), 631–640.

Sirakoulis, G.Ch., Karafyllidis, I., Thanailakis, A., 2000. A cellular automaton model for the effect of population movement and vaccination on epidemic propagation. Ecological Modelling 133 (3), 209–223.

Sirakoulis, G.Ch., Karafyllidis, I., Thanailakis, A., Mardiris, V., 2001. A methodology for VLSI implementation of Cellular Automata algorithms using VHDL. Advances in Engineering Software 32, 189–202.

Sirakoulis, G.Ch., Karafyllidis, I., Thanailakis, A., 2002. A cellular automaton methodology for the simulation of integrated circuit fabrication process. Future Generation Computer Systems 18 (5), 639–657.

Sethian, J.A., 1985. Curvature and evolution of fronts. Communications in Mathematical Physics 101, 487–499.

Tazawa, S., Matsuo, S., Saito, K., 1992. A general characterization and simulation method for deposition and etching technology. IEEE Transactions in Semiconductor Manufacturing 5, 27–36.

Toffoli, T., 1984a. Cellular automata as an alternative to (rather than an approximation of) differential equations in modeling physics. Physica D 10 (1–2), 117–127.

Toffoli, T., 1984b. CAM: a high-performance cellular automaton machine. Physica D 10 (1–2), 195–204.

Ulam, S., 1952. Random processes and transformations. Proceedings of the International Congress on Mathematicians, vol. 2. Cambridge, MA, USA, pp. 264–275.

Vichniac, G.Y., 1984. Simulating physics with cellular automata. Physica D 10 (1–2), 96–116.

von Neumann, J., 1966. Theory of self-reproducing automata. University of Illinois, Urbana.

Weimar, J., Tyson, J.J., Watson, L.T., 1992. Diffusion and wave propagation in cellular automata models of excitable media. Physica D 55, 309–327.

Wilding, N.B., Trew, A.S., Hawick, K.A., Pawely, G.S., 1991. Scientific modeling with massively parallel SIMD computers. Proceedings of the IEEE 79, 574–585.

Wolfram, S., 1986. Theory and Applications of Cellular Automata. World Scientific, Singapore.

Georgios Ch. Sirakoulis was born in Athens, Greece in 1973. He received the Diploma and Ph.D. degrees in Electrical and Computer Engineering from the Democritus University of Thrace, Greece, in 1996 and 2001, respectively. For his Diploma Thesis he received a prize of distinction from the Technical Chamber of Greece (TEE). He has published more than 20 papers in refereed journals and conferences and acts as a referee for several international journals. From 2002 he serves as a lecturer in the Department of Electrical and Computer Engineering, Democritus University of Thrace, Greece. His current research emphasis is on cellular automata theory and applications, bioinformatics, modeling and simulation of microelectronic devices and processes, TCAD, VLSI design applications using VHDL, VLSI physical design, and genetic algorithms. He is a member of the IEEE and of the TEE.

Ioannis Karafyllidis was born in Thessaloniki, Greece in 1959. He received the Dipl. Eng. and Ph.D. degrees in Electrical Engineering from the Aristotle University of Thessaloniki, Greece, in 1983 and 1991, respectively. In 1992 he joined the Department of Electrical and Computer Engineering, Democritus University of Thrace, Greece, as a faculty member, where he is currently an Associate Professor. He has published more than 70 papers in refereed journals and conferences and acts as a referee for several international journals. His current research emphasis is on nanoelectronics, nanotechnology, quantum computing, and cellular automata theory and applications. He is Associate Editor of Current Nanotechnology, a fellow of the Institute of Nanotechnology, a member of the IEEE and a member of the Technical Chamber of Greece (TEE).

Adonios Thanailakis was born in Greece in 1940. He received B.Sc. degrees in physics and electrical engineering from the University of Thessaloniki, Greece, in 1964 and 1968, respectively, and the M.Sc. and Ph.D. degrees in electrical engineering and electronics from UMIST, Manchester, England, UK, in 1968 and 1971, respectively.

He has been a Professor of Microelectronics in the Department of Electrical and Computer Engineering, School of Engineering, Democritus University of Thrace, Xanthi, Greece, since 1977, and he was a visiting Professor in the Departments of Electrical and Computer Engineering, University of Manitoba, Canada, and George Mason University, VA, USA, during the Academic years 1984–1985 and 1996–1997, respectively. He has been active in electronic device research since 1968. His current research activities include amorphous materials and devices, photovoltaic conversion of solar energy, applications of group theory in physical and computational systems, and VLSI systems design. He served as Rector (President) of the Democritus University of Thrace (DUTH), as Dean of the School of Engineering of DUTH, and as Chairman of the Electrical and Computer Engineering Department, School of Engineering of DUTH. He has published a great number of scientific and technical papers, as well as five textbooks on materials, devices, electronic noise, photovoltaic conversion of solar energy, and VLSI systems design. Prof. Thanailakis is a Member of the Institution of Electrical Engineers (IEE), the Institute of Physics (IOP), the European Physical Society (EPS), the Technical Chamber of Greece (TEE), and the Institute of Heliotechnics of Greece (IHT).